ADVANCED MATERIALS
www.advmat.de

High Performance Transmission-Type Daytime Radiative Cooling Film with a Simple and Scalable Method

*Sujin Shao, Siyuan Jia, Xiaofeng Jiang, Pochun Hsu, Wanlin Guo, and Xiuqiang Li**

Transmission-type radiative cooling textiles represent a vital strategy for personal thermal management. However, traditional preparation methods based on heat-induced phase separation face significant challenges regarding cost, environmental impact, and optical performance. Herein, a novel preparation method is devloped by blending mid-IR transparent solid styrene ethylene butylene styrene (SEBS) with solid polyethylene (PE), enabling the creation of pores through dissolving SEBS. Consequently, large-scale production of transmission-type radiative cooling films at the meter scale are achieved, exhibiting 95% solar reflectivity and 80% mid-IR transmittance. Moreover, this method reduces costs by 68% and diminishes CO_2 emissions by 92%. Under sunny and cloudy conditions (solar irradiance ≈730 and 280 Wm^{-2}, respectively), the film-covered simulated skin demonstrates sub-ambient cooling effects of ≈4 and 3 °C. Given its exceptional passive cooling capabilities, low-cost, and scalability, this film holds great potential for industrial and personal applications.

1. Introduction

Nowadays, due to the escalating greenhouse effect, outdoor temperatures during summer continue to rise year after year.[1–3] Exposure to high-temperatures can lead to various health issues such as compromised cardiorespiratory fitness and heat stress in individuals, thereby increasing the risk of mortality.[4–6] This poses significant challenges for both outdoor workers and travelers during the summer season, potentially impacting local economies and cultures in severe cases.[7–9] It is projected that by 2030, the economic repercussions resulting from elevated temperatures will amount to a staggering 2.4 trillion dollars.[10–12] Passive daytime radiative cooling films not only effectively reflect sunlight to mitigate solar heat but also possess the capability of emitting their own energy into outer space for cooling purposes.[13–15] Therefore, they offer a promising solution specifically tailored for outdoor environments where active cooling systems may not be as feasible.[16,17]

Existing daytime radiative cooling films can be classified into two types based on their mechanisms: mid-IR transmission and emission (**Figure** 1a).[18–22] It has been demonstrated that the transmission type reduces thermal resistance in comparison to the emission type for film materials themselves (Figure 1b),[23–25] enabling effective transfer of heat radiation from the human body to achieve efficient body cooling. Currently, the predominant type of transmission-based radiative cooling films is porous polyethylene (PE), which is fabricated via heat-induced phase separation.[26–28] Specifically, PE is blended with paraffin oil and subsequently extruded to form films or fibers.[29–31] The formation of pores is achieved by dissolving the paraffin oil (Figure S1, Supporting Information). However, due to issues such as incomplete removal of pore-forming agents and non-uniform mixing of these agents, the sunlight reflectivity of currently available meter-scale PE materials is ≈55% (Figures S2 and S3, Supporting Information). Additionally, the preparation process is highly polluting and costly.

In this study, we have developed a preparation method by blending mid-IR transparent solid Styrene Ethylene Butylene Styrene (SEBS) with solid polyethylene (PE) to create pores through the dissolution of SEBS. This method streamlines the technological process by allowing partial retention of the pore-forming agent while avoiding its contamination (compared to paraffin oil-based preparation methods), and correspondingly improves the production yield (relative to the previous solid-solid preparation approach).[32] Leveraging these advantages, we have fabricated meter-scale daytime radiative cooling films that exhibit over 95% solar reflectivity and more than 80% mid-IR transmittance. Additionally, the cost has been reduced by 68%, and CO_2 emissions have been decreased by 92%. Experimental results demonstrate that our film can maintain a temperature more than 8 °C lower than conventional cotton textile under sunny conditions, effectively safeguarding human health in high-temperatures. In sunny and cloudy weather (solar irradiance ≈730 and 280 W m^{-2}), our film can achieve sub-ambient cooling of ≈4 and 3 °C, respectively. Compared with currently reported transparent materials, our film demonstrates

---

S. Shao, S. Jia, X. Jiang, W. Guo, X. Li
Key Laboratory for Intelligent Nano Materials and Devices of Ministry of Education, and International Institute for Frontier Science
Nanjing University of Aeronautics and Astronautics
Nanjing 210016, China
E-mail: xiuqiang.li@nuaa.edu.cn

P. Hsu
Pritzker School of Molecular Engineering
University of Chicago
Chicago, IL 60637, USA

The ORCID identification number(s) for the author(s) of this article can be found under https://doi.org/10.1002/adma.202511138

DOI: 10.1002/adma.202511138

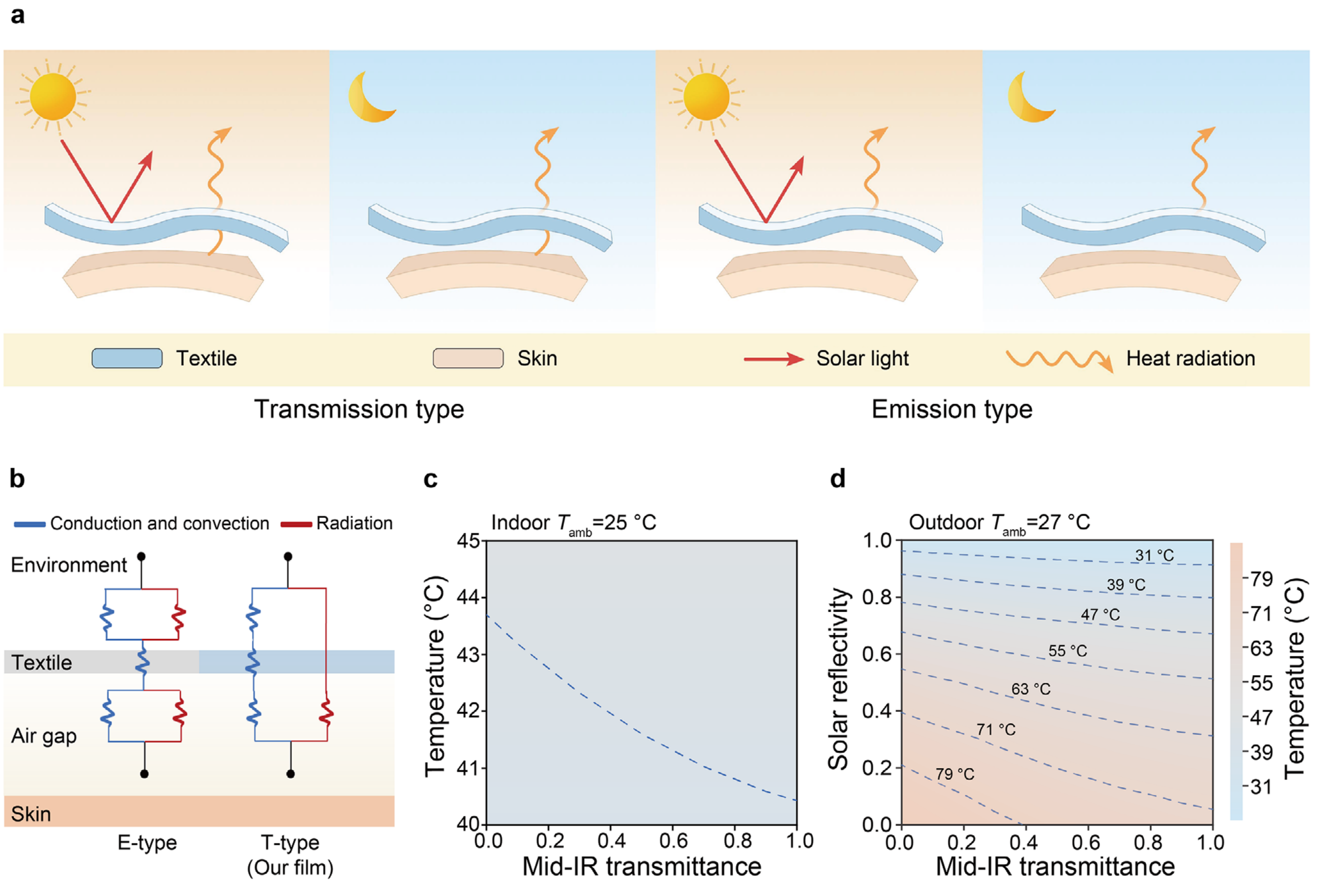

Figure 1. Comparison and calculation of emission and transmission films. a) Schematic illustration of body heat output and solar heat input for mid-IR transmission and emission film. b) Schematic analysis of the heat resistance of emission-type film versus transmission-type film (our film). c) and d), Skin temperatures calculated for different types of films covered in indoor versus outdoor conditions. Using steady state heat transfer model, the human body has a steady metabolic generation rate (140 W m^{-2}), the indoor environment has a constant temperature (25 °C), while the outdoor environment also has a constant temperature (27 °C) and sufficient sunlight (800 W m^{-2}).

comprehensive advantages in optical performance, environmental impact, and cost-effectiveness (Table S1, Supporting Information).

2. Results and Discussion

2.1. Heat Transfer Model Calculations

We evaluated the indoor and outdoor cooling performance of films with varying solar reflectivity and mid-infrared (mid-IR) emissivity, including emission-type films ($\varepsilon_{ir} = 1$) and transmission-type film (PE, $\tau_{ir} = 1$), using steady-state heat transfer models (see Note S1 and Table S2 and Figures S4 and S5, Supporting Information).[33–35] As shown in Figure 1c, the simulated skin temperature increases with higher emissivity. Transmission-type films demonstrate better cooling performance indoors at 25 °C, with a 3.3 °C lower temperature than emission-type films. Under outdoor conditions with an irradiance of 800 W m^{-2}, the surface temperature of skin covered by transmission-type films is 3.5 –14 °C lower than that covered by emission-type films when both have identical solar reflectivity (Figure 1d). Additionally, solar reflectivity significantly influences the cooling properties of films in outdoor settings. For instance, for transmission-type films, the simulated skin temperature is 8.6 °C lower at 100% solar reflectivity compared to 90%. It is evident that in outdoor sunlight, transmission-type films exhibit superior cooling performance relative to emission-type films, with a more pronounced temperature reduction as solar reflectivity increase. Both indoor and outdoor simulations confirm that transmission-type films possess superior heat transfer capabilities and outstanding cooling performance compared to emission-type films.

2.2. Material Design and Characterization

In the preparation of film material, the conventional heat-induced phase separation method is replaced with solid-solid blend phase separation (**Figure 2a**). Specifically, we utilize mid-IR transparent PE as the base material and select mid-IR transparent SEBS as a pore-forming agent (see Note S2 and Figure S6, Supporting Information for more controlled experiments). The two materials are mixed using a twin-screw extruder and then heat-pressed into a membrane (Figure S7, Supporting Information). After removing SEBS from the membrane using

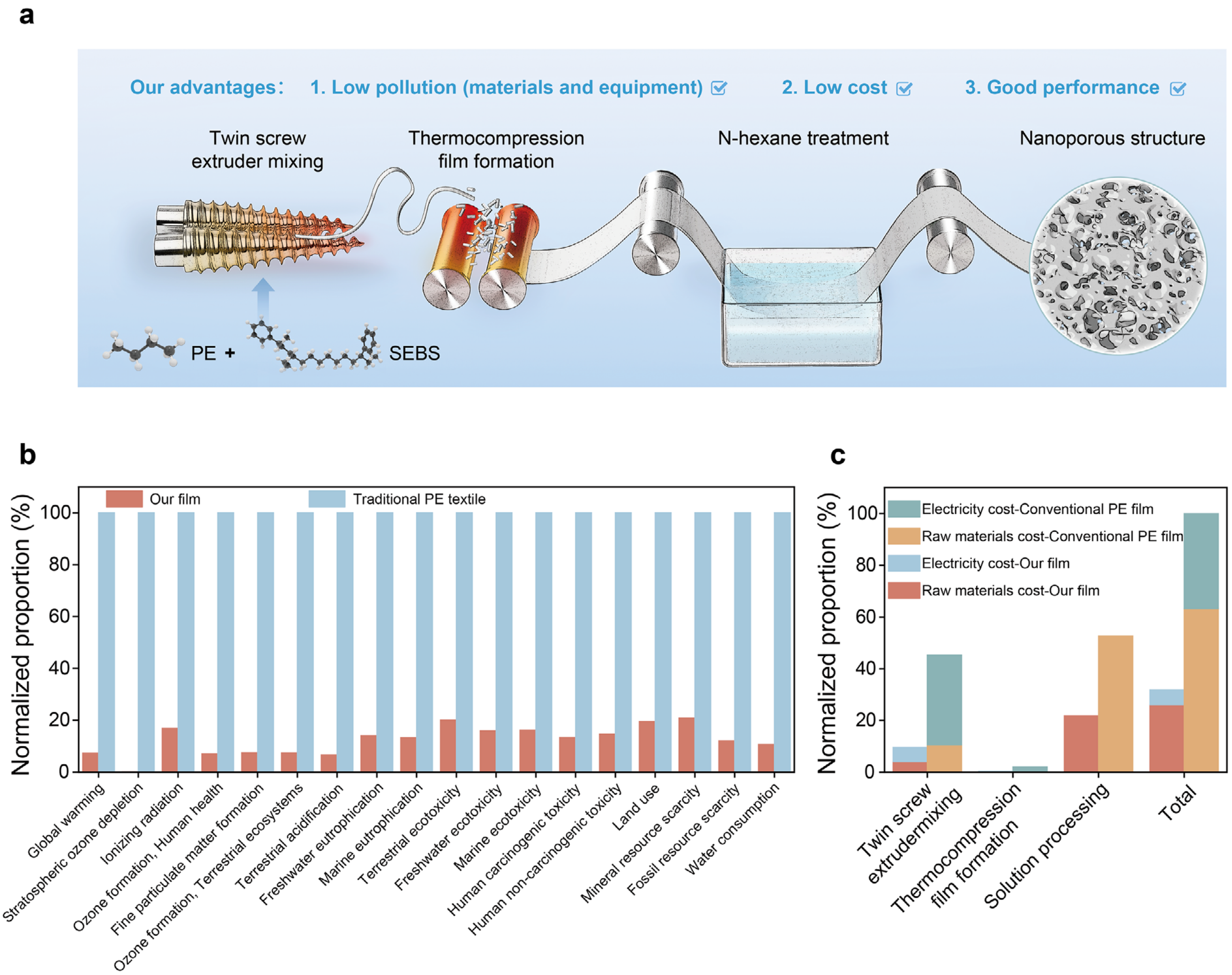

Figure 2. Preparation of the materials. a) Preparation process of our film. b) Life cycle environmental impacts of our film compared to conventional PE. c) Cost comparison between our film and conventional PE in terms of raw material and energy consumption.

n-hexane at 60 °C, a porous structure with a white smooth appearance on macroscopic scale is formed (Figure S8, Supporting Information). As our material consists of two solid-phase materials instead of PE blended with paraffin oil, it allows SEBS to partial remain. This innovative methodology effectively addresses two critical limitations inherent in conventional PE film fabrication processes. First, it significantly reduces environmental contamination by eliminating the oxidation risks and pore-forming agent residue issues associated with paraffin oil utilization in conventional pore-forming approaches. Second, it demonstrates remarkable process efficiency through simplified post-treatment – our optimized procedure requires merely a single-step cleaning protocol for complete removal of pore-forming agent, in stark contrast to the conventional method's requirement for multiple washing cycles to ensure thorough paraffin oil elimination. It's worth noting that when n-hexane dissolves with SEBS cools down to room temperature, SEBS solidifies and precipitates out, enabling recycling and reusing n-hexane. To rigorously quantify the comparative benefits of the solid-solid blend phase separation methodology, we conducted a systematic evaluation encompassing both environmental footprint and economic viability through two key analytical dimensions: (1) lifecycle assessment (LCA) using mass-energy balance calculations, and (2) comprehensive cost-benefit analysis incorporating material and energy inputs (all data from laboratory scale).

Life cycle assessment (LCA), defined as a systematic methodology for evaluating environmental impacts and associated resource flows throughout the life cycle of a product or service system (ISO 14040, 14044), was employed in this study (see Note S3 and Tables S3–S5, Supporting Information for more details). A comparative assessment was established between the life cycle environmental impacts of producing 1 kg of our novel material and conventional PE, with detailed system boundaries illustrated in Figures S9 and S10 (Supporting Information). As demonstrated in Figure 2b, the novel preparation method we developed is significantly reduced in all types of environmental impacts compared to the conventional PE preparation method, in particular, the CO_2 emission equivalent is reduced by ≈92% (see Figures S11 and S12, Supporting Information for more comparative data). This is due to the much smaller amount of our

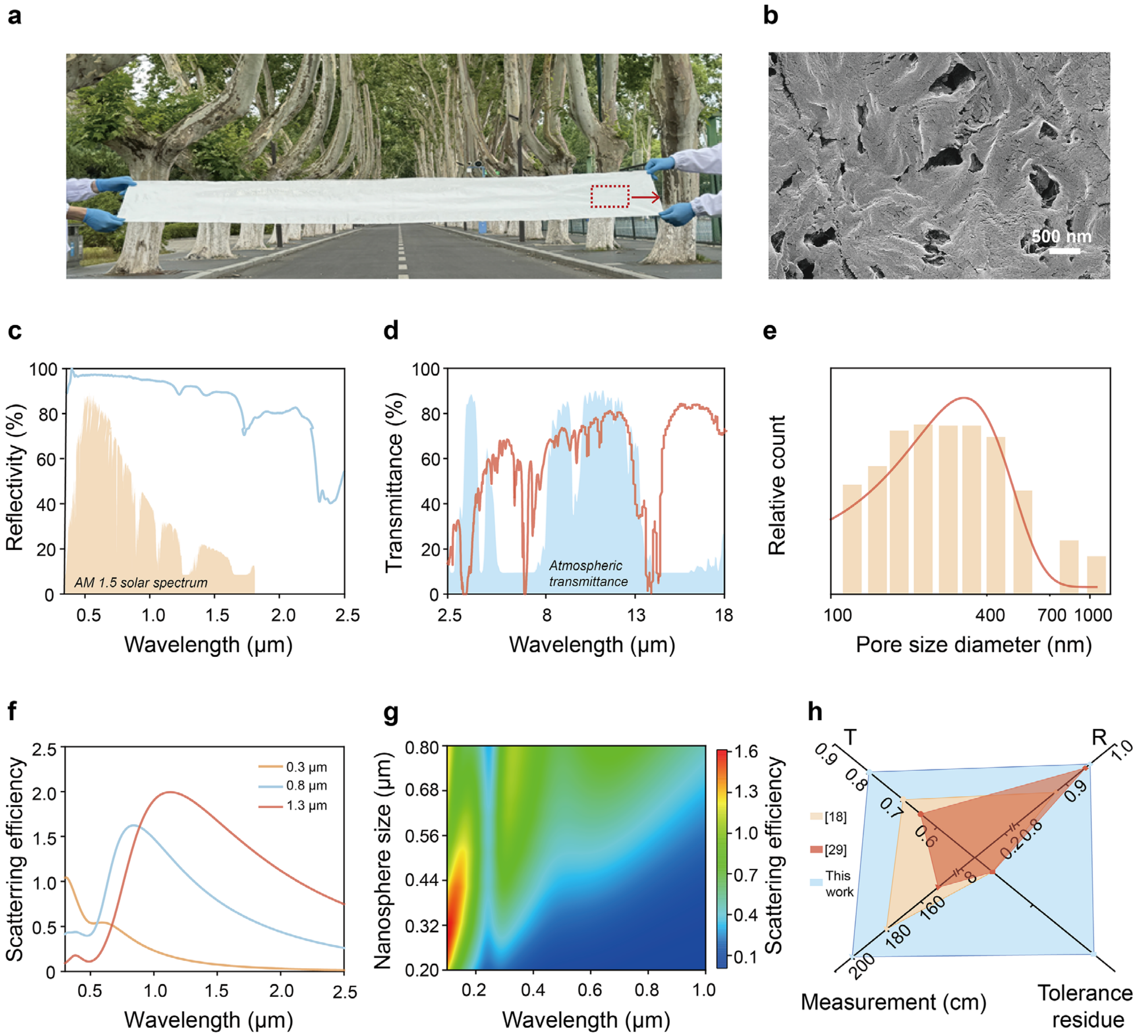

Figure 3. Optical properties of materials. a) Optical photograph of our film (0.2 by 2 m). b) High-resolution SEM image of our film. It has micropores at the nanometer level. c) Reflectivity of the UV–vis–NIR spectrum (0.34-2 μm). d) Transmittance of the mid-IR spectrum (2.5–18 μm) measured by an integrating sphere. The shaded regions show the AM 1.5G solar spectrum (yellow) and atmospheric transmittance (blue) for reference.[36] e) Pore diameter distribution of our film. The diameter of the nanopores is only 30 to 1100 nm, which is the key to ensuring high solar reflectivity and high mid-IR transmittance. f) Scattering efficiency in the range of 0.1–2.5 μm of the nanopores (0.3, 0.8, and 1.3 μm). g) Scattering efficiency in the 0.1–1 μm wavelength range for nanopores with diameters of 0.2–0.8 μm in the material calculated from FDTD (Finite Difference Time Domain) simulations. h) Comparison of this work with previously reported work includes four items: solar reflectivity (*R*), mid-IR transmittance (*T*), measurement, and whether or not to allow for residuals of the pore-making agent.[27,40]

solid-phase pore-forming agent and the higher yield resulting from the allowance of residues.

Figure 2c demonstrated significant cost advantages of our method in raw materials and electricity consumption, with production costs at 197 CNY kg^{c} versus 616 CNY/kg for the conventional approach, representing a 68% reduction in cost (see Note S3, Tables S6–S8, Supporting Information for more details). Although our laboratory-scale costs remain considerable, strategic scaling would substantially reduce expenses, confirming enhanced economic viability and sustainability. Thanks to these advantages, we achieve meter-scale preparation of daytime radiative cooling film (**Figure** 3a,b).

To further enhance the solar reflectivity of the film, we initially investigated the impact of the PE and SEBS mixing ratio on its solar reflectivity (Figure S13, Supporting Information). The addition of SEBS increased solar reflectivity; however, when the ratio of PE to SEBS reached 3:7, it caused breakage in the n-hexane-treated samples. Consequently, a PE to SEBS ratio of 4:6 was chosen. Furthermore, we optimized the thickness considering that increasing it would negatively affect mid-IR transmittance while enhancing solar reflectivity (Figures S14 and S15, Supporting Information). Therefore, a thickness of 165 µm was selected for the film. Lastly, we also optimized the dissolution time of SEBS. It was observed that after 1.25 h of treatment in n-hexane, both solar reflectivity and mid-IR transmittance remained stable without any further improvement with increased treatment time (Figure S16, Supporting Information). Thus, a n-hexane treatment time of 1.25 h was determined.

After the above optimization, the film we prepared exhibits a high reflectivity of 95% in the sunlight spectrum (0.4–2.5 µm) and a high transmittance of 80% in the heat radiation spectrum of the human body (8–13 µm) (Figure 3c,d). These findings suggest that our film can effectively prevent overheating from solar radiation outdoors while facilitating heat transfer, which accounts for over 60% of the body's thermal exchange, to the environment.[37] In an effort to investigate the underlying reasons behind our film's exceptional solar reflectivity, we employed Mie scattering theory and simulated it using FDTD.[38,39] According to Mie scattering theory, materials exhibit significant scattering efficiency when their micropore diameter distribution closely aligns with specific wavelength bands. As depicted in Figure 3e,g, since our film possesses a microporous aperture distribution within the ultraviolet to near-infrared waveband range, its reflectivity within this range is significantly enhanced. Additionally, due to smaller apertures compared to mid-IR wavelengths, there is lower Mie scattering efficiency in this range favoring higher transmittance (Figure S17, Supporting Information). Furthermore, the porosity (the volume fraction of scatterers) directly impacts the solar scattering efficiency. By controlling the blending ratio of SEBS (Figure S8, Supporting Information), we achieved regulation of the porosity. When a blend ratio of 60 wt.% SEBS and 40 wt.% PE was used, the post-treated film attained a porosity of 17%. FDTD simulations confirmed that this condition yields the peak solar scattering efficiency for the film (Figure S18, Supporting Information). The pore size of 500 nm being much smaller than mid-IR wavelengths ensures that porosity modulation primarily affects solar-band scattering characteristics while having negligible impact on mid-IR transmittance performance. We have also compared our film's performance with previous literatures, as illustrated in Figure 3h, highlighting several advantages including: 1) High solar reflectance (95%); 2) High mid-IR transmittance (80%); 3) Large size (>2 m); 4) Capability to retain pore-making agent residue thereby reducing preparation costs and pollution.[27,40]

2.3. Indoor Thermal Measurements

To assess the cooling performance of our film, we have developed an in-house heat flux test platform (**Figure 4**a; FigureS19, Supporting Information) to measure cooling power, along with foam insulation chambers (thermocouples were attached to the simulated skin to measure its temperature). To minimize solar absorption and convection heat loss, all components were placed inside a silver-coated foam chamber with PE film cover to evaluate temperature change.[41] The additional cooling power required to achieve a skin temperature of 34 °C using different textiles (our film, cotton, nylon, and polyester) under a light exposure of 500 Wm^{-2} indoors were measured (Figure 4b). The result showed that our film exhibited negligible additional cooling power compared to cotton (67.85 Wm^{2}), nylon (121.66 Wm^{-2}), and polyester (73.97 Wm^{-2}). As shown in Figure 4c, the skin covered by our film is ≈6 °C cooler than bare skin and 2–5 °C cooler than other textiles. Additionally, we have selected several types of PE with varying solar reflectivity (Figure S2, Supporting Information) for comparison with our film. The solar reflectivity of PE1-3 gradually increased by 55.2%, 79.5%, and 89.5%, respectively. As observed in Figure S20a (Supporting Information), as the sunlight reflectivity increased, the additional cooling requirement to maintain a simulated skin temperature of 34 °C decreased significantly from 93.69 Wm^{-2} (PE1), 93.47 Wm^{-2} (PE2), and 25.85 Wm^{-2} (PE3) to only 2.56 Wm^{-2} in our sample under an irradiance of light at 500 Wm^{-2}. As shown in Figure S20b (Supporting Information), the temperature of our film-covered skin in the chamber was also ≈1–4 °C lower than the other three types of PE. It can be observed that during indoor tests, not only does our designed film exhibit superior performance compared to mainstream textiles but it also outperforms some low-reflective PE materials.

2.4. Outdoor Thermal Measurements

After conducting indoor testing to evaluate the performance of our film, we proceeded to investigate its outdoor radiative cooling capabilities under different weather conditions (sunny, cloudy) in Nanjing, China. The experimental setup (Figure 4d; Figure S21, Supporting Information) with various types of textiles (including our film, cotton, nylon, and polyester) on a simulated skin (made of silicone rubber) surface were placed outdoor for testing. Real-time temperatures of the simulated skin were recorded from 10:00 to 16:00. As depicted in Figure 4e,g, during sunny outdoor conditions with a peak solar irradiance of 930 Wm^{-2} (relative humidity: 35%), our film achieved an average temperature of only 34 °C for the covered simulated skin area, resulting in a sub-ambient cooling effect of ≈4 °C (the average ambient temperature on the day was ≈38 °C). Notably, its temperature was the lowest of all the samples, measuring 8.3, 15.4, and 9.8 °C lower than the simulated skin temperatures covered by cotton, nylon, and polyester, respectively, even farther below the bare skin temperature (17.3 °C). Under cloudy outdoor conditions (relative humidity: 60%), our film also exhibited effective cooling performance. The average temperature of the simulated skin covered by our film was 27 °C, which is 3 °C lower than the average ambient temperature (30 °C) during the testing period (Figure 4e,h,i). The simulated skin temperature of its covered was 2.9 °C (cotton), 6.2 °C (nylon), 3.7 °C (polyester), and 7.1 °C (bare skin) lower than that of the other textiles covered, respectively. In addition, nighttime measurements conducted from 20:00 to 06:00 demonstrate our film achieved 5 °C sub-ambient cooling (simulated skin: 25 °C) at a mean ambient temperature of 30 °C (Figure S22, Supporting Information). We also evaluated the outdoor radiative cooling performance of nanoporous PE with varying solar reflectivity. The differences in solar reflectivity had an even greater impact on the cooling performance under solar illumination. Despite our film having lower mid-IR transmittance compared to PE1 (Figure S2, Supporting Information), it still achieved a skin temperature reduction of 3.8 °C

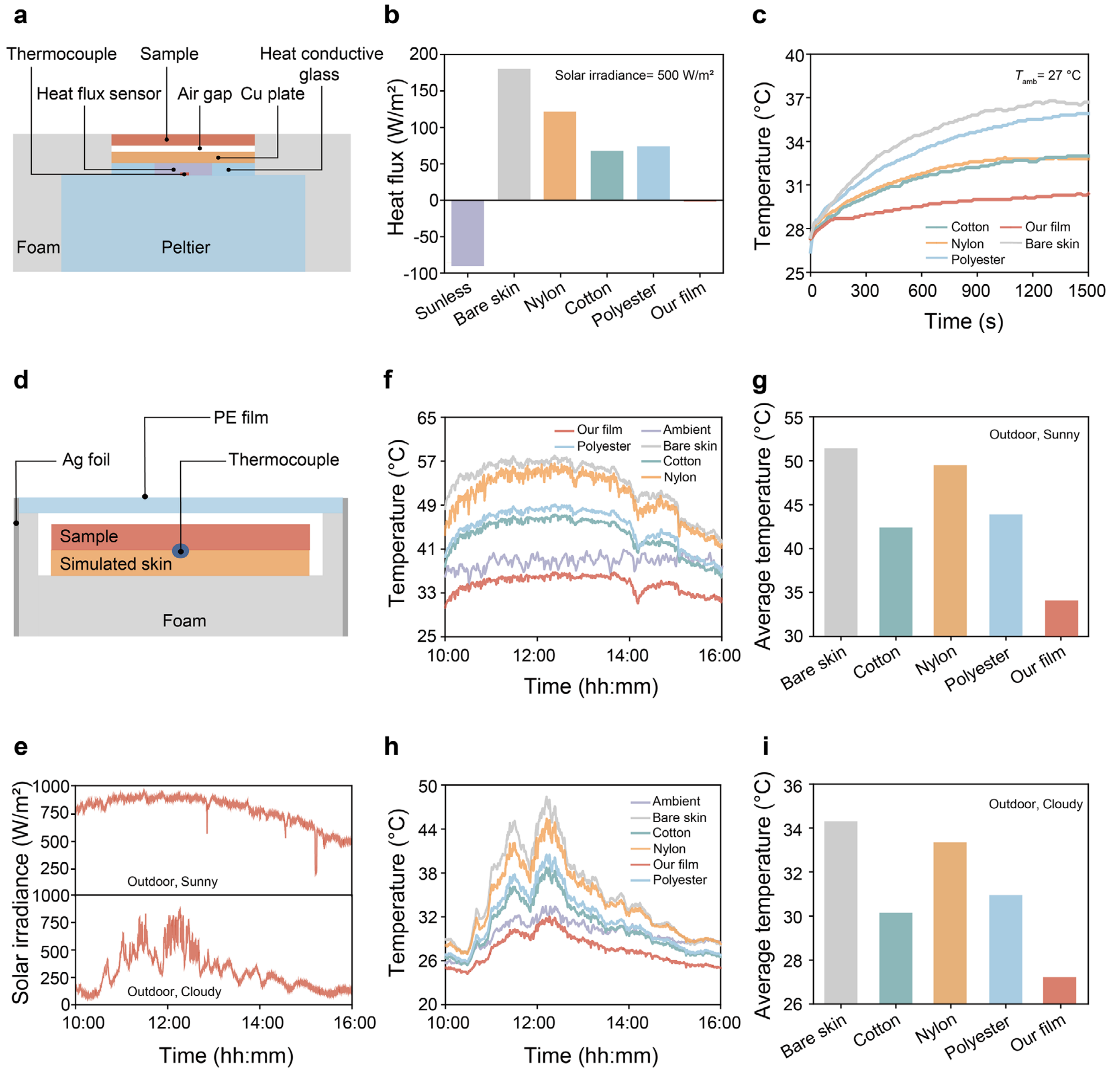

Figure 4. Thermal testing indoors and outdoors. a) Schematic diagram of the self-constructed indoor heat flow test platform. b) Additional cooling power required to reach 34 °C for simulated skin covered by our film, cotton, polyester, nylon, and simulated skin alone under 500 W m^{-2} simulated solar irradiation. c) Temperature of simulated skin covered by our film, cotton, polyester, and nylon with simulated skin itself under 500 W m^{-2} simulated solar irradiation. d) Schematic diagram of the device for testing the effectiveness of films cooling outdoors. e) The day's real-time solar irradiance. The upper part is under sunny condition (24 May 2024) and the lower part is under cloudy condition (21 May 2024). f,g) Tests under sunny condition. h,i) Tests under cloudy conditions. (f) and (h) Real-time temperature of simulated skin covered by different textiles and real-time air temperature. (g) and (i) Average temperature of simulated skin covered by different textiles.

compared to PE1, as well as 7.2 °C and 1.9 °C lower than PE2 and PE3, respectively, due to its higher solar reflectivity (Figure S23, Supporting Information). Our film consistently exhibited significantly lower simulated skin temperatures in all conditions, showcasing its superior cooling ability attributed to its high solar reflectivity that minimizes heat input from the sun while maximizing radiation heat output through efficient transmission of body heat.

2.5. Wearability and Application

To assess the actual performance of our film in terms of wearability, we opted for a protective clothing as the control group and affixed our film on the right side of the back of the suit (the corresponding area where the suit's original textile had been excised), while retaining the suit's original textile on the left side for comparison purposes (**Figure** 5a–c). Under three distinct testing

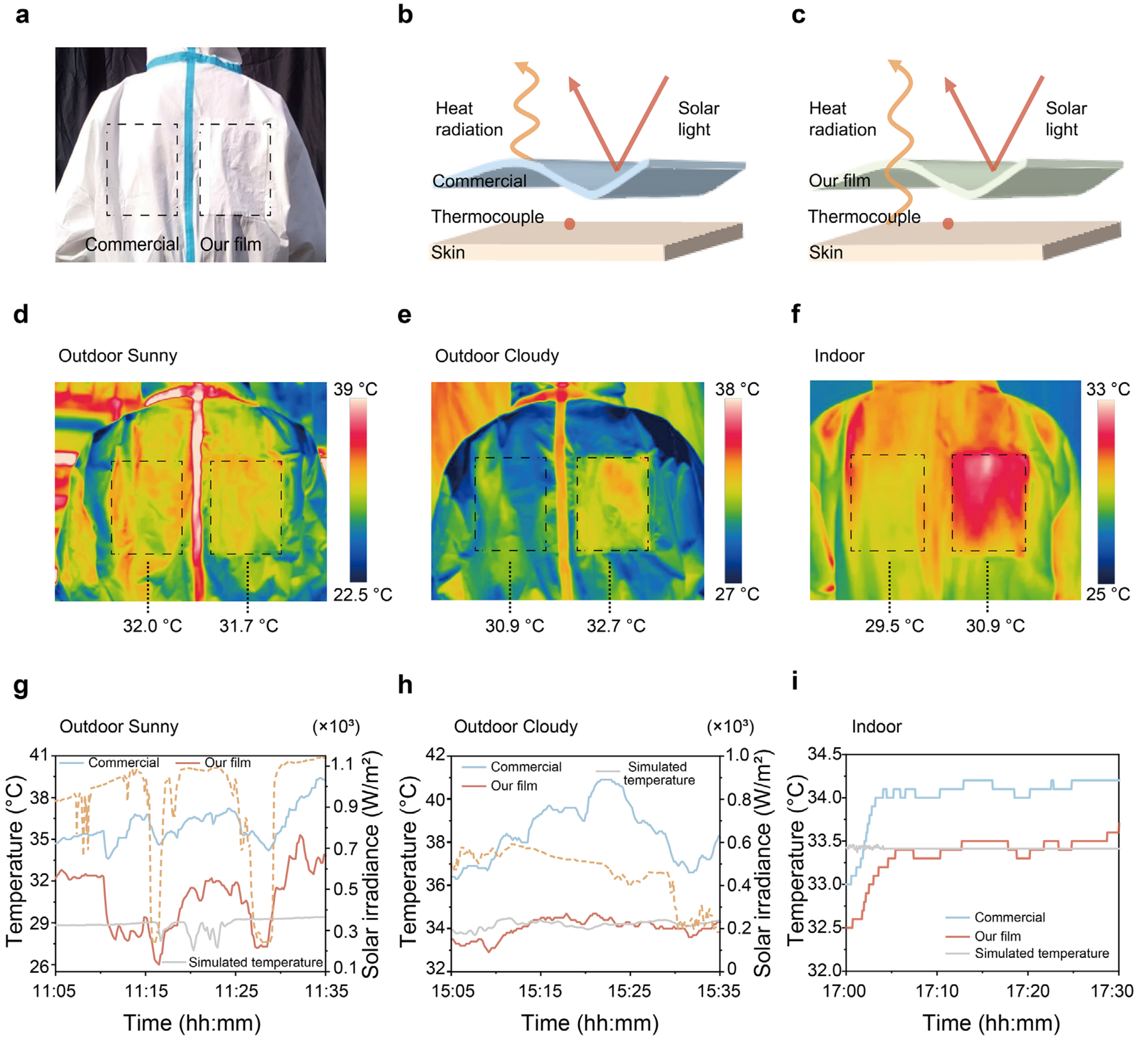

Figure 5. Testing of our film under human wear conditions. a) Optical photograph of protective clothing. Commercial protective clothing textile is on the left, and our film is on the right. b) and (c) Schematic of commercial protective clothing textile on the left and our film on the right. d), e), and f) Infrared images of experimenters wearing protective suits (commercial suit on the left and our film on the right) with the average temperature of the framed area at 30th min under outdoor sunny (23 September 2024), cloudy (25 September 2024), and indoor (24 September 2024) conditions. g), h), and i) Real-time measurements and simulations of film-covered skin temperature and instantaneous solar irradiance (orange dashed line) were conducted under three environmental conditions: sunny outdoors, cloudy outdoors, and indoors.

conditions: outdoor sunny, outdoor cloudy, and indoor settings, we meticulously captured infrared images and monitored temperature fluctuations (measured via thermocouples positioned beneath both textiles and attached to the skin) on both sides of the experimenter's back.

As depicted in Figure 5d, under outdoor sunny conditions, our film exhibited a higher apparent temperature (31.3 °C) compared to the commercial protective clothing (30.4 °C) due to its high mid-IR transmittance. Over time, both the suit and the body reached thermal equilibrium under solar heating, causing the textiles on both sides of the back to converge at the same temperature as observed through infrared imaging. However, owing to our film's superior solar reflectivity, thermocouple measurements beneath it (Figure 5g) revealed that the skin covered by our film had a temperature ≈5 °C lower than that covered by commercial protective clothing. The measured temperature of our film exhibited an ≈2 °C deviation from the simulated values (see Note S1; Table S9, Supporting Information). This discrepancy may be attributed to the influence of outdoor atmospheric humidity and airborne pollutants, which could potentially compromise the film's radiative cooling efficiency and lead to localized heat accumulation. During cloudy outdoor conditions, infrared images consistently showed a temperature drop of ≈2 °C for our film compared to commercial textile due to its excellent infrared transmission capability (Figure 5e). This pattern was also confirmed by thermocouple-measured temperatures (Figure 5h), demonstrating favorable performance in outdoor radiative cooling for our film with a consistent 5 °C temperature reduction, matching the simulated temperature trend. In a 28 °C indoor environment, our film demonstrates a 0.7 °C cooling effect compared to commercial protective clothing, in line with simulation data (Figure 5f,i). However, when solely employing infrared cameras for measurement purposes, our film consistently exhibited an approximate elevation of 1.4 °C compared to commercial protective clothing. It follows that our film has a better infrared transmission capacity, which allows for a better transmission of body heat radiation into the environment. To sum up, the film we have developed exhibits exceptional outdoor and indoor cooling performance, thereby significantly enhancing human comfort.

To ensure optimal wearing comfort, we enhanced the breathability and water permeability of the film using a 30G microneedle perforation technique. As shown in Figure S24a,b (Supporting Information), reducing the perforation distance significantly increased water permeability, reaching 385.54 g m^{-2}·day at a distance of 1 mm, while its optical properties remain essentially unchanged. However, its water permeability remains significantly lower than the moisture permeability achievable with fiber structures.[42] Textile weaving-inspired structural designs offer potential for further property enhancement.

Durability evaluation, as a critical aspect of functional textile assessment, was systematically investigated in this study. We subjected our film to one hundred wash cycles and examined any changes in its optical properties (Figure S24c, Supporting Information). The results revealed an 8% decrease in solar reflectivity after one hundred washes compared to the unwashed condition, yet the structural integrity remained unaffected. Furthermore, our film exhibits excellent tensile strength for daily wear (Figure S24d, Supporting Information). Finally, we evaluated the long-term outdoor stability of our film through accelerated aging tests.[43–46] As shown in Figure S25 (Supporting Information), after 160 h of aging, no characteristic absorption peaks related to oxidation processes were observed,[47–50] and the surface oxygen content remained essentially unchanged, indicating no significant oxidation occurred in our film. Remarkably, the film showed minimal variations in key optical performance parameters, with solar reflectivity fluctuations within 1.8% and mid-IR transmittance changes below 2.5%.

3. Conclusion

In summary, we have developed a novel method for the preparation of hierarchically porous PE through solid-solid blending of SEBS and PE, followed by dissolving SEBS. After optimizing the parameters of the preparation process, we have successfully achieved large-scale production of transmission-type radiative cooling films that exhibit a solar reflectivity of 95% and mid-IR transmission of 80%. Additionally, the cost has been reduced by 68%, and CO_2 emissions have been decreased by 92%. Experiments have proven that under sunny conditions, our film is more than 8 °C cooler than conventional cotton textile, effectively safeguarding human health in high-temperatures. Moreover, the results show that our film can achieve sub-ambient cooling of ≈4 °C and 3 °C in sunny and cloudy weather respectively. In future studies, fiber-like samples will be prepared to enhance wearing comfort and expand application possibilities.

Supporting Information

Supporting Information is available from the Wiley Online Library or from the author.

Acknowledgements

National Natural Science Foundation of China (5230130227), Fundamental Research Funds for the Central Universities (NS2023060), Key Research and Development Program of Jiangsu Province (BE2023815), NUAA (Nanjing University of Aeronautics and Astronautics) Startup Fund (4017-YQR22012), Jiangsu Specially-Appointed Professors.

Conflict of Interest

The authors declare no conflict of interest.

Author Contributions

X.L. conceived the idea, designed the experiments, and supervised the research project. S.S., S.J., and X.J. conducted the experiments. S.S. performed the simulation. S.S. analyzed the data and wrote the paper. All authors contributed to the experiments and discussion of the manuscript.

Data Availability Statement

The data that support the findings of this study are available in the supplementary material of this article.

Keywords

fabrication method, personal thermal management, polyethylene, radiative cooling film

Received: June 12, 2025
Revised: August 26, 2025

---

[1] J. N. Munday, *Joule* **2019**, *3*, 2057.
[2] M. N. Cramer, D. Gagnon, O. Laitano, C. G. Crandall, *Physiol. Rev.* **2022**, *102*, 1907.
[3] Y. Wang, X. Zhang, S. Liu, Y. Liu, Q. Zhou, T. Zhu, Y.-E. Miao, N. Willenbacher, C. Zhang, T. Liu, *Adv. Mater.* **2024**, *36*, 2400102.
[4] K. L. Ebi, A. Capon, P. Berry, C. Broderick, R. de Dear, G. Havenith, Y. Honda, R. S. Kovats, W. Ma, A. Malik, N. B. Morris, L. Nybo, S. I. Seneviratne, J. Vanos, O. Jay, *Lancet* **2021**, *398*, 698.
[5] J. I. Halonen, A. Zanobetti, D. Sparrow, P. S. Vokonas, J. Schwartz, *Environmental health* **2010**, *9*, 42.

[6] Y. Wang, S. Liu, X. Zhang, Y. Liu, T. Zhu, B. Ji, J. Chen, Y. Cheng, W. Fan, Y.-E. Miao, N. Willenbacher, C. Zhang, T. Liu, *ACS Nano* **2025**, *19*, 19328.

[7] B. Jones, B. C. O'Neill, L. McDaniel, S. McGinnis, L. O. Mearns, C. Tebaldi, *Nat. Clim. Change* **2015**, *5*, 652.

[8] C. He, Y. Zhang, A. Schneider, R. Chen, Y. Zhang, W. Ma, P. L. Kinney, H. Kan, *Nat. Commun.* **2022**, *13*, 3847.

[9] Y. Xie, Z. Zhou, Q. Sun, M. Zhao, J. Pu, Q. Li, Y. Sun, H. Dai, T. Li, *iScience* **2024**, *27*, 109066.

[10] *DARA and the Climate Vulnerable Forum, Climate Vulnerability Monitor: A Guide to the Cold Calculus of a Hot Planet*, 2nd ed., (Ed: M. McKinnon), DARA, Madrid, Spain, **2012**.

[11] J. Sun, Y. Zhang, Y. Wang, Y. Peng, J. Long, H. Liu, W. Fan, Y.-E. Miao, N. Willenbacher, C. Zhang, T. Liu, *Adv. Funct. Mater.* **2025**, *35*, 2425527

[12] E. Pennisi, *Science* **2020**, *370*, 778.

[13] P.-C. Hsu, A. Y. Song, P. B. Catrysse, C. Liu, Y. Peng, J. Xie, S. Fan, Y. Cui, *Science* **2016**, *353*, 1019.

[14] X. Yin, R. Yang, G. Tan, S. Fan, *Science* **2020**, *370*, 786.

[15] P.-C. Hsu, X. Li, *Science* **2020**, *370*, 784.

[16] D. Li, X. Liu, W. Li, Z. Lin, B. Zhu, Z. Li, J. Li, B. Li, S. Fan, J. Xie, J. Zhu, *Nat. Nanotechnol.* **2021**, *16*, 153.

[17] D. E. Abraham, R. Yang, J. Mandal, M. Yore, X. Huang, V. K. Turner, W. Wells, K. Schwarz, D. P. Eisenman, A. P. Raman, *Nat. Sustain.* **2025**, *8*, 642.

[18] Y. Peng, Y. Cui, *Joule* **2020**, *4*, 724.

[19] Q. Zhang, S. Wang, X. Wang, Y. Jiang, J. Li, W. Xu, B. Zhu, J. Zhu, *Small Methods* **2022**, *6*, 2101379.

[20] Z. Li, W. Chen, *Mater. Chem. Front.* **2021**, *5*, 6315.

[21] S. Zeng, S. Pian, M. Su, Z. Wang, M. Wu, X. Liu, M. Chen, Y. Xiang, J. Wu, M. Zhang, Q. Cen, Y. Tang, X. Zhou, Z. Huang, R. Wang, A. Tunuhe, X. Sun, Z. Xia, M. Tian, M. Chen, X. Ma, L. Yang, J. Zhou, H. Zhou, Q. Yang, X. Li, Y. Ma, G. Tao, *Science* **2021**, *373*, 692.

[22] R. Wu, C. Sui, T.-H. Chen, Z. Zhou, Q. Li, G. Yan, Y. Han, J. Liang, P.-J. Hung, E. Luo, D. V. Talapin, P.-C. Hsu, *Science* **2024**, *384*, 1203.

[23] P. C. Hsu, C. Liu, A. Y. Song, Z. Zhang, Y. Peng, J. Xie, K. Liu, C.-L. Wu, P. B. Catrysse, L. Cai, S. Zhai, A. Majumdar, S. Fan, Y. Cui, *Sci. Adv.* **2017**, *3*, 1700895.

[24] L. Cai, A. Y. Song, P. Wu, P.-C. Hsu, Y. Peng, J. Chen, C. Liu, P. B. Catrysse, Y. Liu, A. Yang, C. Zhou, C. Zhou, S. Fan, Y. Cui, *Nat. Commun.* **2017**, *8*, 496.

[25] B. Zhu, W. Li, Q. Zhang, D. Li, X. Liu, Y. Wang, N. Xu, Z. Wu, J. Li, X. Li, P. B. Catrysse, W. Xu, S. Fan, J. Zhu, *Nat. Nanotechnol.* **2021**, *16*, 1342.

[26] A. Leroy, B. Bhatia, C. C. Kelsall, A. Castillejo-Cuberos, M. Di Capua H, L. Zhao, L. Zhang, A. M. Guzman, E. N. Wang, *Sci. Adv.* **2019**, *5*, aat9480.

[27] Y. Peng, J. Chen, A. Y. Song, P. B. Catrysse, P.-C. Hsu, L. Cai, B. Liu, Y. Zhu, G. Zhou, D. S. Wu, H. R. Lee, S. Fan, Y. Cui, *Nat. Sustain.* **2018**, *1*, 105.

[28] N. Guo, L. Yu, C. Shi, H. Yan, M. Chen, *Nano Lett.* **2024**, *24*, 1447.

[29] L. Cai, Y. Peng, J. Xu, C. Zhou, C. Zhou, P. Wu, D. Lin, S. Fan, Y. Cui, *Joule* **2019**, *3*, 1478.

[30] J. Zhang, Z. Zhou, J. Quan, D. Zhang, J. Sui, J. Yu, J. Liu, *Sol. Energy Mater. Sol. Cells* **2021**, *225*, 111029.

[31] M. Yang, W. Zou, J. Guo, Z. Qian, H. Luo, S. Yang, N. Zhao, L. Pattelli, J. Xu, D. S. Wiersma, *ACS Appl. Mater. Interfaces* **2020**, *12*, 25286.

[32] E. Torgerson, J. Hellhake, *Sol. Energy Mater. Sol. Cells* **2020**, *206*, 110319.

[33] L. Cai, A. Y. Song, W. Li, P.-C. Hsu, D. Lin, P. B. Catrysse, Y. Liu, Y. Peng, J. Chen, H. Wang, J. Xu, A. Yang, S. Fan, Y. Cui, *Adv. Mater.* **2018**, *30*, 1802152.

[34] X. Wu, J. Li, Q. Jiang, W. Zhang, B. Wang, R. Li, S. Zhao, F. Wang, Y. Huang, P. Lyu, Y. Zhao, J. Zhu, R. Zhang, *Nat. Sustain.* **2023**, *6*, 1446.

[35] S. Shao, L. Yuan, X. Li, W. Guo, *Next Energy* **2024**, *2*, 100083.

[36] *Standard Tables for Reference Solar Spectral Irradiances: Direct Normal and Hemispherical on 37° Tilted Surface*, ASTM International, West Conshohocken, PA, **2012**.

[37] J. D. Hardy, E. F. Dubois, *Proc. Natl. Acad. Sci. USA* **1937**, *23*, 624.

[38] J. Mandal, Y. Fu, A. C. Overvig, M. Jia, K. Sun, N. N. Shi, H. Zhou, X. Xiao, N. Yu, Y. Yang, *Science* **2018**, *362*, 315.

[39] N. Cheng, D. Miao, C. Wang, Y. Lin, A. A. Babar, X. Wang, Z. Wang, J. Yu, B. Ding, *Chem. Eng. J.* **2023**, *460*, 141581.

[40] T. Wang, X. Wu, Q. Zhu, Y. Chen, S. Zhang, M. Gu, Y. Zhang, *Nanophotonics* **2024**, *13*, 601.

[41] X. Li, B. Sun, C. Sui, A. Nandi, H. Fang, Y. Peng, G. Tan, P.-C. Hsu, *Nat. Commun.* **2020**, *11*, 6101.

[42] M. Alberghini, S. Hong, L. M. Lozano, V. Korolovych, Y. Huang, F. Signorato, S. H. Zandavi, C. Fucetola, I. Uluturk, M. Y. Tolstorukov, G. Chen, P. Asinari, R. M. Osgood, M. Fasano, S. V. Boriskina, *Nat. Sustain.* **2021**, *4*, 715.

[43] J. Song, W. Zhang, Z. Sun, M. Pan, F. Tian, X. Li, M. Ye, X. Deng, *Nat. Commun.* **2022**, *13*, 4805.

[44] H. Zhang, J. Zhang, J. Chen, X. Hao, S. Wang, X. Feng, Y. Guo, *Polym. Degrad. Stab.* **2006**, *91*, 2761.

[45] D. Grossman, W. Ketola, *Accelerated and Outdoor Durability Testing of Organic Materials*, ASTM International, Pennsylvania, USA, **1994**.

[46] C.-H. Zhang, Y.-D. Huang, W.-J. Yuan, J.-N. Zhang, *J. Appl. Polym. Sci.* **2011**, *120*, 2468.

[47] L. E. P. Real, *Weathering of Polymers and Plastic Materials*, 1st ed., Springer Nature, Cham, Switzerland **2023**.

[48] I. H. Craig, J. R. White, *J. Mater. Sci.* **2006**, *41*, 993.

[49] M. Li, C. Lin, K. Li, W. Ma, B. Dopphoopha, Y. Li, B. Huang, *Small* **2023**, *19*, 2301159.

[50] M. Nichols, *Coatingstech* **2020**, *17*, 18.